*The paper was presented at the Eleventh Meeting*
*"New Trends in Fatigue and Fracture" (NT2F11)*
*Polignano a Mare, Italy, 3–6 July, 2011*

*Akram Alhussein[1], Julien Capelle[1], Joseph Gilgert[1], Serge Dominiak[2], Zitouni Azari[1]*

# INFLUENCE OF SANDBLASTING AND HYDROGEN ON TENSILE AND FATIGUE PROPERTIES OF PIPELINE API 5L X52 STEEL

# UTICAJ PESKIRANJA I VODONIKA NA ZATEZNE OSOBINE I ZAMOR API 5L X52 ČELIKA ZA CEVOVOD

Originalni naučni rad / Original scientific paper
UDK /UDC: 620.17 : 621.643
Rad primljen / Paper received: 9.10.2011

Adresa autora / Author's address:
[1)] Laboratoire de Mécanique, Biomécanique, Polymère, Structures (LaBPS), Ecole Nationale d'Ingénieurs de Metz – Université Paul Verlaine de Metz, Metz, France, akrmanh@hotmail.com
[2)] Laboratoire de Physique Mécanique Matériaux (LPMM), Ile du Saulcy, Metz, France

**Keywords**
- pipeline
- sandblasting erosion
- electrolytic hydrogen
- mechanical properties
- FAD
- API 5L X52

**Ključne reči**
- cevovod
- erozija peskiranjem
- elektrolitički vodonik
- mehaničke osobine
- FAD
- API 5L X52

*Abstract*

*The evaluation of static properties and lifetime of a pipeline notched under the impact of sand with or without the presence of hydrogen has been performed. The material damage is made by electrolytic hydrogen and projecting corundum particles (aluminium oxide). It is shown that sandblasting and hydrogen have little effect on the yield stress and ultimate strength. The material lifetime and elongation at fracture are clearly affected by hydrogen, which penetrates into the surface layers of the material and changes the local fracture mechanism. Despite the erosion of these layers, under the sand impacting, failure strain and lifetime are improved. The observation of failure mode shows that the deformation field, after sandblasting, is very important. The crack propagation and the failure seem to be intragranular. The cracks, in the pipeline API 5L X52 steel charged with hydrogen, propagate following the porosity path without any distinct direction. The absorbed hydrogen atoms placed inside the crystalline sites of steel cause the embrittlement of material so that a small effort is sufficient to create cleavage. Modified notch failure assessment diagram is used to evaluate the risk of studied notch defect in different environments: air, hydrogen and sandblasting.*

*Izvod*

*Izvedena je procena statičkih osobina i veka cevovoda sa zarezom nastalim udarom peska sa ili bez prisustva vodonika. Oštećenje materijala izvedeno je elektrolitičkim vodonikom i snopom čestica korunda (oksida aluminijuma). Pokazuje se da peskiranje i vodonik imaju malog uticaja na napon tečenja i čvrstoću. Vek materijala i izduženje pri lomu su jasno pod uticajem vodonika, koji prodire u površinske slojeve materijala i menja lokalni mehanizam loma. Uprkos eroziji ovih slojeva, pod udarima peska, dolazi do povećanja lomne deformacije i veka. Posmatranje oblika loma pokazuje da je deformaciono polje, posle peskiranja, od izuzetnog značaja. Širenje prsline i lom deluju interkristalno. Prsline, u cevovodu od čelika API 5L X52 sa vodonikom, se šire prateći poroznost bez nekog jasnog pravca. Apsorbovani atomi vodonika smešteni unutar lokacija kristala u čelika izazivaju krtost materijala tako da je za pojavu cepanja dovoljno i manje naprezanje. Upotrebljen je modifikovani dijagram procene loma sa zarezom za procenu rizika proučene greške tipa zareza u različitim uslovima sredine: vazduh, vodonik i peskiranje.*

## INTRODUCTION

Erosion is a mechanical process that causes an eroded volume on the surface of a material. The erosion phenomenon of metallic structures, in petroleum industry, subjected to fatigue process by sandblasting, is a problem that affects many industrial sectors. The shocks between the sand particles and the structure surface cause a severe damage. It is manifested by spalling craters of different shapes and depths, /1/. The wall-thickness is gradually reduced and the rupture occurs when the stresses in the crater reaches a limiting threshold.

The erosion rate increases according to the sandblasting duration up to a constant value, Hattori and Nakao /2/.

These authors divide the phenomenon of the eroded volume into four consecutive stages: the initial stage characterized by high volume loss rate at the beginning of the test, the incubation stage (some cracks are observed because of the accumulating plastic deformation), the acceleration stage and the maximum rate stage where the original surface is completely removed.

The main parameters of erosion are: the exposure time, the kinetic energy of particles (erosion rate is proportional to the mass and velocity of sand particles) /3, 4/, and the impact angle (the maximum erosion rate depends on the material behaviour, /5/). Irrespective of the impact loading type (solid particles, Hopkinson bar, impact fatigue, ...etc.), the materials stresses, strains, and damaged surfaces would increase with increase of the impact velocity, /3, 6, 7/.

The mechanical, chemical and thermal actions are the cause of material separation, but the means to achieve these actions are different. According to Meng and Ludema /8/, there are four main mechanisms of erosion by impact of solid particles, Fig. 1.

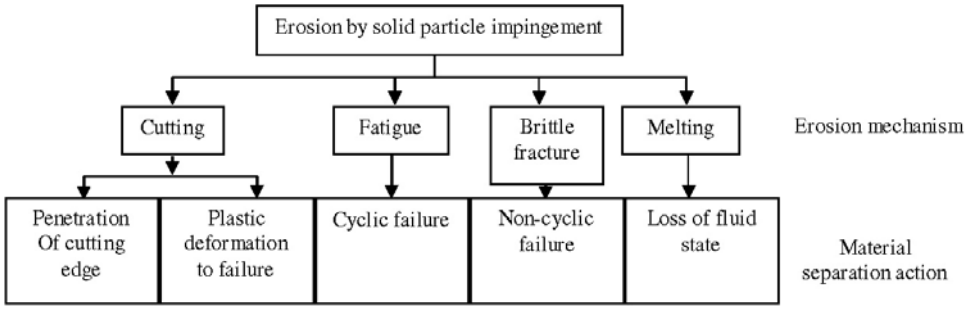


Figure 1. Mechanism of solid particle erosion, /8/.
Slika 1. Mehanizam erozije čvrstim česticama, /8/

In order to study the material lifetime after the sandblasting operation, many fatigue tests are made. The sand erosion process improves resistance to fatigue under stresses, /9, 10, 11/. This improvement comes from the introduction of residual stresses in compression at the hardened surface layers. Many studies show the benefits of the process on the material fatigue. De Los Rios /12/ and Vo /13/ show an improvement of endurance limit and material lifetime. This improvement is due to the surface state which improves by limiting the micro concentrations of stresses. This allows a larger cleavage time.

In the present paper, the hydrogen influence on the behaviour law and lifetime of the pipeline API 5L X52 steel is studied. Many studies worldwide have indicated the technical feasibility of the use of hydrogen as an energy carrier in the transport and energy sectors, /14, 15, 16/. Hydrogen, being the smallest atom identified, can move easily in the crystalline sites of steel. The hydrogen diffuses in steel according to the traditional mechanisms of hetero diffusion at infinite dilution, /17/.

According to Sofronis /18/, in the presence of hydrogen, the yield stress increases slightly with hydrogen concentration. He proposes a linear evolution of the yield stress with the hydrogen concentration. Delafosse and Magnin /19/ show (for a pipeline X52 steel) that the yield stress is slightly affected by the presence of electrolytic hydrogen. Only the failure strain is dramatically reduced by hydrogen action. Failure occurs in air for an elongation of about 28%, while in a severe concentration of electrolytic hydrogen (test potential of –1700 $mV_{SCE}$), it appears for an elongation of 3.5%. They also conclude that the ultimate strength varies very little.

The hydrogen influence on material plasticity is expressed by one of the following hypothesis:

1 – The atomic cohesion forces

Two models dealing with the hydrogen effects on cohesion forces are proposed by Troiano /20/ and Oriani /21/. These models assume a local decrease of the atomic network cohesive forces, due to the presence of hydrogen in the matrix or at grain boundaries /22/ (or any other metallurgic defect). A crack can propagate when the applied tensile stress is sufficient to counterbalance the cohesion force of the network, modified by the hydrogen presence.

In reality, Qiao /23/ shows that the high concentration of hydrogen, located at the crack tip in XC80 steel, is sufficient to get a rupture by cleavage. This model is particularly interesting in the case of centred cubic metals (CC), which can cleave very easily. It has been shown that the hydrogen absorption allows ductile fracture behaviour to be a brittle one /24, 25/.

2 – Initiation and propagation of cracks

Delafosse and Magnin /19/, Mao and Li /26/, show that the effect of crack creation can't be only linked to the presence of hydrogen, particularly in the networks with centred cubic faces (CCF). Nothing, until now, allows to identify the hydrogen responsibility percentage at a crack initiation. As against, if the crack is already formed, its propagation will be amplified.

3 – Hydrogen trapping by dislocations

The transport phenomenon by dislocations, /27/, forming the basis of certain mechanisms of embrittlement, assume the existence of a hydrogen trapping by dislocations and the transport accelerated of the hydrogen atoms by moving dislocations.

Bastien and Azou /28/ are the first who suggest that "hydrogen–dislocation" interactions are involved in the mechanisms of embrittlement by hydrogen. This mechanism, based on the fact that hydrogen as a proton, could be transported by the dislocations and thus contributes to the creation of a micro-crack at a level of dislocations stacking.

This requires that the protons can follow the moving dislocations. To do this, it is imperative that the diffusion velocity of protons is greater than or equal to the dislocations movement velocity.

For a hydrogen concentration in a specimen with X46 steel, loaded by three points bending test, and for different bending moments, it has been shown that the area of high stresses (in the middle of specimen) is highly charged with hydrogen. The dislocations in large numbers in this area play a role of traps for hydrogen.

## EXPERIMENTAL PROCEDURE

### *Material*

Mechanical tests are realized on specimens with API 5L X52 steel taken from a tube in both directions, Fig. 2: longitudinal direction (L), transverse direction (T). This tube has an external diameter of 610 mm and a thickness of 11 mm. It is used in the European natural gas transporting network. This section was removed from a pipeline in the beginning of this century. It therefore represents the actual European transport network.

The pipe is manufactured according to the standards of the American Petroleum Institute: API 5L X52. The chemical composition of this steel is presented in Table 1.

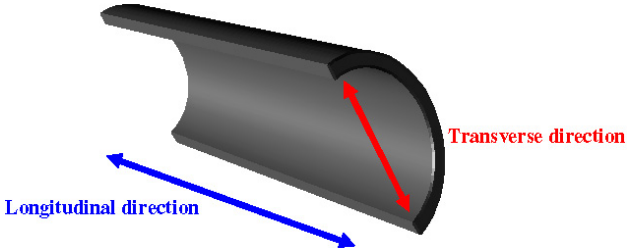


Figure 2. Longitudinal and transverse directions of pipeline.
Slika 2. Podužni i poprečni pravci cevovoda

Table 1. Chemical composition of pipeline API 5L X52 steel (wt %).
Tabela 1. Hemijski sastav čelika cevovoda API 5L X52 (tež. %)

| C | Mn | Si | Cr | Ni | Mo | S | Cu | Ti | Nb | Al |
|---|---|---|---|---|---|---|---|---|---|---|
| 0.206 | 1.257 | 0.293 | 0.014 | 0.017 | 0.006 | 0.009 | 0.011 | 0.001 | <0.03 | 0.034 |

The microstructure of API 5L X52 steel is analysed by optical microscopy after mechanical polishing and chemical treatment with Nital, Fig. 3.

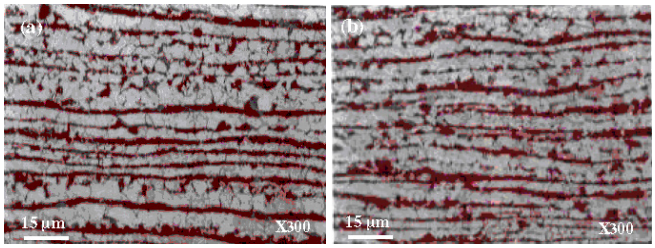


Figure 3. Microstructure of pipeline API 5L X52 steel: a) Longitudinal analysis, b) Transverse analysis.
Slika 3. Mikrostruktura čelika cevovoda API 5L X52: a) podužna analiza, b) poprečna analiza

Metallographic analysis confirms that the sheet used in the manufacture of this pipe is rolled in both directions (longitudinal and transverse). The rolling rate in both directions may be different. Indeed, we observe bands of pearlite coloured in black alternating with bands of ferrite in white which is a sign of rolling. We can also say that the ferrite is the main component of this structure. The microstructural study shows that the grain diameters range from 7 to 15 µm.

### *Sandblasting conditions*

The basis of this study is to assess the material damage by sand impacting. For this purpose, we used a Blaster 2700 sandblasting machine, equipped with a pressure gauge, enabling it to adjust the desired power, Fig. 4. Sand supply ($Al_2O_3$) is ensured by the venturi effect, with a constant sand feed throughout sandblasting operation. The air flow velocity (32 $ms^{-1}$) is measured by means of a wind gauge using an anemometer. It represents the average wind velocity or the sandblasting velocity in nature (especially in the desert regions). It is evident that the flux velocity obtained by the anemometer does not correspond to the sand particle velocity. The sand particle velocity is not determined because of the complexity related to the variations in the nature, size and shape of sand. Sand grains have an angular shape and their average size is between 300 and 400 µm. The physical and mechanical properties of the sand are respectively presented in Tables 2 and 3.

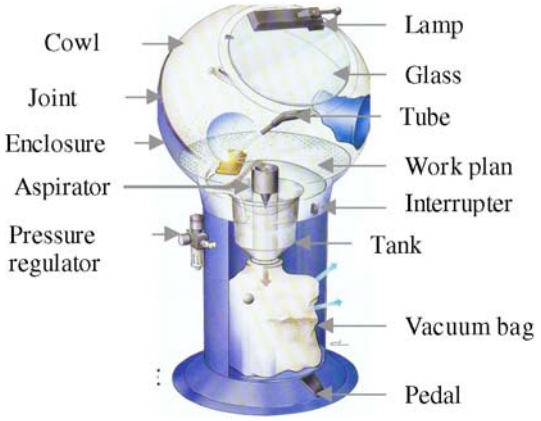


Figure 4. Blaster 2700 Sandblasting machine.
Slika 4. Mašina za peskiranje Blaster 2700

Table 2. Physical properties of sand (corundum).
Tabela 2. Fizičke osobine peska (korund)

| Composition $Al_2O_3$ | Density ($g/cm^3$) | Water absorption rate (%) |
|---|---|---|
| >99.9% | 3.95 | 0 |

Table 3. Mechanical properties of sand (corundum) in air, /42/.
Tabela 3. Mehaničke osobine peska (korunda) na vazduhu, /42/

| Hardness Vickers (HV) | Tensile strength ($N/mm^2$) | Bending strength ($N/mm^2$) | Compression strength ($N/mm^2$) | Young modulus ($N/mm^2$) | Poisson's ratio | Fracture toughness ($MPa \cdot m^{1/2}$) |
|---|---|---|---|---|---|---|
| 1800-2000 | 200-250 | 200-600 | 1900-2000 | $3.8 \cdot 10^5$ | 0.25-0.3 | 4-5 |

In order to adjust the projection angle of the abrasive and to concentrate the particle impact on a predefined area, an assembly is made, Fig. 5, with the following properties: nozzle diameter of 8 mm, an average sand feed during the erosion tests is about 1.57 $gs^{-1}$, an impact angle between the sand particles and the specimen surface is 90°, a distance between the nozzle and the specimen is 200 mm (allowing sand particles to impact all the notched area), an air pressure of 4 bar and sandblasting duration of 8 hours.

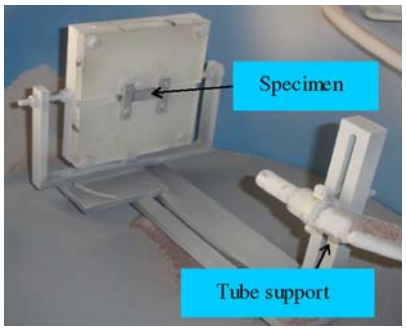


Figure 5. Specimen holder assembly.
Slika 5. Sklop držača epruvete

*Damage conditions by hydrogen*

Hydrogen in its gaseous state ($H_2$) is found in rare percentage on Earth. It is generally (99.98% of cases) recombined with other atoms in various materials (oil, water, metals, ...etc.). To obtain the hydrogen, different methods are used. In our study, the hydrogen is produced by electrolysis of water ($H_2O$). The water used must be very pure (deionised) to avoid the disruption of electrolysis operation by impurities. At room temperature and up to 80°C /29, 30/, electrolysis dissociates the water molecules into two constituent atoms: oxygen and hydrogen, and introduces hydrogen at the electrode, which will be the loading specimen.

The charging cell under electrolytic hydrogen, for tensile and fatigue tests, consists of two parts:

– A first box of homogenization, where the $CO_2$ and $N_2$ gas bubbles are made to stabilize the pH solution and to take off dissolved oxygen respectively.
– A second box called "hydrogen-charging" contains the reference calomel electrode, the auxiliary electrode with platinum and working electrode, which in our case, corresponds to the specimen, Fig. 6.

To ensure the homogeneity of the NS4 solution (Table 4), a pump circulates the electrolytic solution box by box.

Typically, the electrolysis cell consists of two electrodes (cathode and anode), an electrolyte and a current generator. The chosen electrolyte is a proton exchange membrane. We have the following anode and cathode reactions in respect:

$$H_2O \rightarrow 2H^+ + 1/2O_2 + 2e^-$$

$$2H^+ + 2e^- \rightarrow H_2$$

In order to perform an electrolysis process, it is necessary to have an external power source allowing an electron transfer reaction. A potentiostat will be used as a current source. It provides the capability to electronically regulate the current to get the fixed potential.

The free potential (potential with the absence of external current) on the polarization curve of our steel is –0.79 $V_{SCE}$. This value complies with the literature /31/ for this type of steel. To realize a reduction (cathode reaction), we apply a potential lower than this free potential value. Tests under electrolytic hydrogen will be realized at a constant potential of –1 $V_{SCE}$, and in a standard electrolytic solution: NS4 (Natural Soil 4), for which the characteristics are given in Table 4.

Table 4. Chemical composition of NS4 solution (milligram/litre).
Tabela 4. Hemijski sastav rastvora NS4 (mg/l)

| KCl | $NaHCO_3$ | $CaCl_2$, $2H_2O$ | $MgSO_4$, $7H_2O$ |
|---|---|---|---|
| 122 | 483 | 181 | 131 |

Electrolysis realization requires multiple electrodes, Fig. 6, /32, 33/:

– Reference electrode is a saturated calomel electrode. It is used to control the applied tension.
– Auxiliary electrode is made of stainless steel (platinum). It is used to measure the evolution of current during the test.
– Working electrode is the specimen (hydrogen atoms are adsorbed on the surface of the specimen and with time they can diffuse towards interior of the specimen).

The pH solution is automatically controlled between 6.6 and 6.8. These values correspond to the pH of the soil (about 6.7). To keep this value during all the tests, we introduce discontinuous $CO_2$ gas bubbles by means of an optional rate valve, controlled with an automaton.

During the electrolysis process, the aqueous solution produces oxygen. In order to deaerate the electrolytic solution, continuous nitrogen bubbles ($N_2$) are provided.

The charging cell with electrolytic hydrogen and its various components are presented in Fig. 6. For electrolytic hydrogen charging and any type of the test realized (tensile or fatigue test), we use the parameters defined above.

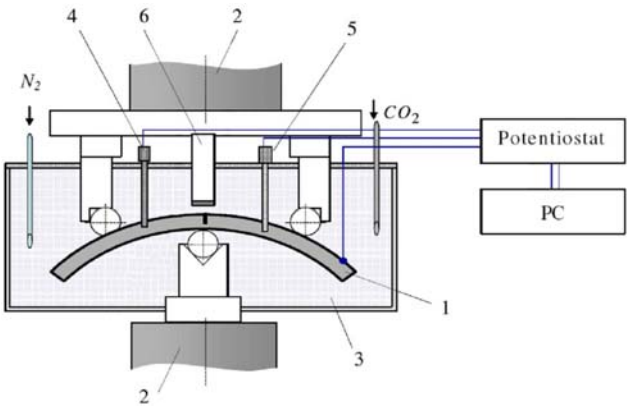


Figure 6. Schematic view of electrolysis cell: 1-"Roman tile" specimen; 2-loading device of testing machine; 3-corrosion cell with NS4 solution; 4-pH electrode; 5-reference calomel electrode; 6-auxiliary electrode.
Slika 6. Shema ćelije za elektrolizu: 1-epruveta tipa „Rimska ploča"; 2-uređaj za zadavanje opterećenja; 3-koroziona ćelija sa NS4 rastvorom; 4-pH elektroda; 5-referentna kalomel elektroda; 6-pomoćna elektroda

## RESULTS AND DISCUSSIONS

*Static characteristics*

The behaviour law of the material is obtained by performing tensile tests on specimens taken from a pipeline in both L and T directions. The specimen geometry is presented in Fig. 7. These specimens are flat with a rectangular section. Its dimensions fit with the European standard NF EN 10002-1, /34/. Moreover, the extraction and manufacturing of specimens is carried out so that the area (of the neutral plane) of a tube coincides with that of tensile specimens.

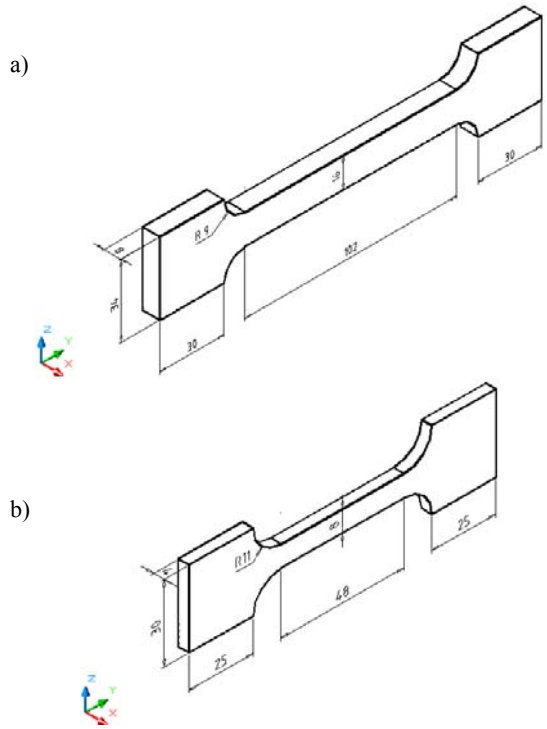


Figure 7. Tensile specimen geometry: a) L direction, b) T direction.
Slika 7. Geometrija zatezne epruvete: a) podužna, b) poprečna

These tests are performed on the machine INSTRON 5585H (Fig. 8), equipped with a static load cell of ±250 kN, pneumatic jaws and a bidirectional video extensometer which controls tensile strain, /34/.

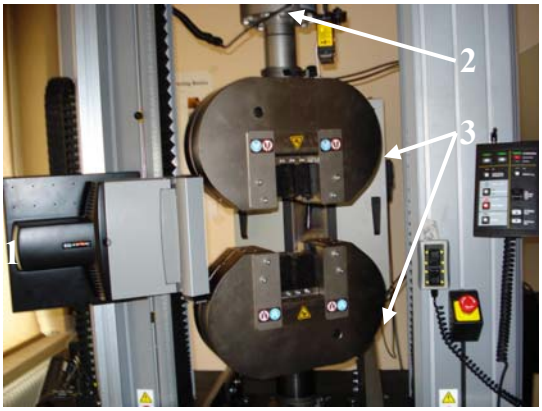


Figure 8. Tensile/compression machine: INSTRON 5585H: 1-video extensometer; 2-load cell; 3-jaws.
Slika 8. Mašina za zatezanje/pritisak: INSTRON 5585H: 1-video ektenzometar; 2-ćelija za opterećenje; 3-čeljusti

a) In the longitudinal direction (L):

Tensile tests are realized on four specimens (L) of identical geometry: two original specimens treated as a reference, the other two impacted by sandblasting for eight hours; sanding is applied to one of the two specimen's faces.

b) In the transverse direction (T):

Tests are performed on eight specimens (T) of identical geometry: three reference specimens, three sandblasted for eight hours (sandblasting is applied to one of the two surfaces of the specimen) and two specimens charged with electrolytic hydrogen for hundred hours. The only useful zone, determined in the middle of the specimen (8 mm × 8 mm), is charged with hydrogen. All other specimen surfaces are covered with anticorrosion paint, based on epoxy.

The material damage, by sandblasting and hydrogen, is carried out for 8 and 100 hours, respectively. Beyond these values, the damaging variation is little.

The stress strain curves, Fig. 9, represent one test of each configuration. The average values of all tests are presented in Table 5.

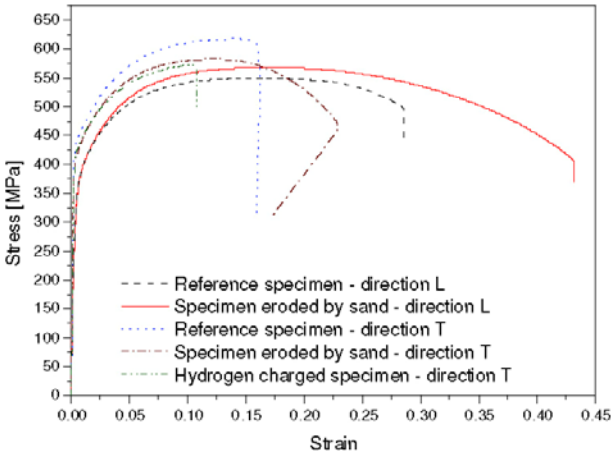


Figure 9. Behaviour law of API 5L X52 steel in L and T directions.
Slika 9. Zakon ponašanja čelika API 5L X52 za oba pravca L i T

Table 5. Influence of sandblasting and hydrogen on the tensile properties of pipeline API 5L X52 steel in both directions: L and T.
Tabela 5. Uticaj peskiranja i vodonika na zatezne osobine čelika API 5L X52 za cevovod u oba pravca: L i T

| Specimen type | Yield stress $\sigma_y$ (MPa) | | Ultimate strength $\sigma_u$ (MPa) | | Elongation at fracture, A% | |
|---|---|---|---|---|---|---|
| | L | T | L | T | L | T |
| Reference | 318 | 450 | 548 | 626 | 24.94 | 18.17 |
| Impacted by sand | 322 | 429 | 561 | 574 | 34 | 21.23 |
| Charged by hydrogen | – | 420 | – | 570 | – | 10.56 |

In view of these results, it is possible to conclude that:

1–Pipeline API 5L X52 steel without pre-mechanical loading (reference specimens) is more resistant in the T than in the L direction. This behaviour is due to the ferrite and pearlite bands, which are more compressed in the T direction. This effect is produced during manufacturing of the pipe (rolling and welding).

2–The material behaviour in both L and T directions, after eight hours of sandblasting, is different:

a) In the L direction, the sandblasting increases all the static mechanical characteristics. The increase of yield stress and ultimate strength is slight but the elongation at fracture is very large. It is about 36% more compared to reference specimens. Sand particles, impacting the surface layers of pipeline, decrease the porosity and increase the material ductility which improves the failure strain.

b) In the T direction, sandblasting reduces yield stress by 4.7% and the ultimate strength by 8.3% while fracture strain is increased by 16.8%.

c) In both L and T configurations, the influence of sandblasting on the static properties of the material is expressed by the increase of elongation at rupture. This advantage is

due to the plastification of the surface layers impacted by sand, which increases material ductility.

3–In the presence of hydrogen, all tensile properties are lowered. The yield stress and ultimate strength are decreased by a small quantity, about 6.7% to 8.9% respectively. On the other side, the elongation at fracture is considerably reduced as it can be seen in Table 5. Its obvious reduction (42%) is due to hydrogen absorption. Its presence, inside steel, modifies the stress strain behaviour of the material. Material fracture behaviour changes from ductile to brittle.

*Fatigue characteristics*

The purpose of these tests is to show the simultaneous influence of sandblasting and hydrogen on the lifetime of a notched pipe. Defects (notch, crack, ...etc.) in a pipe surface are considered as the origin of failures in service. Several studies have focused on the determination of deformation, near external defects, in a pressurised cylindrical shell /35, 36, 37/. In this work, several fatigue tests (3-point bending tests) on Roman tile specimens are performed. These specimens are taken in the transverse direction (T). The thickness corresponds to that of the pipe and the width is 15 mm, Fig. 10. For each specimen, a notch is made by electro-erosion in the external surface of the pipe, Fig. 10. The V-notch shape is chosen to avoid scratches due to machining. These specimens are not standardized. Pipe dimensions do not allow using standard specimens.

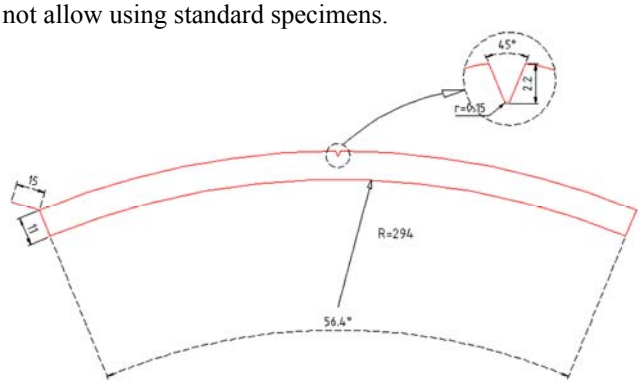


Figure 10. Fatigue specimen geometry: “Roman tile” specimen.
Slika 10. Geometrija zamorne epruvete: „Rimski crep“

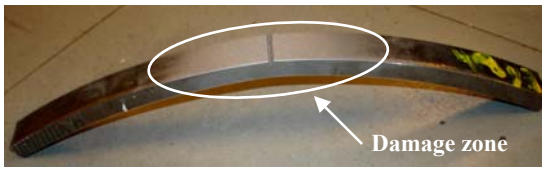


Figure 11. Specimen sandblasted during eight hours.
Slika 11. Uzorak peskiran tokom osam sati

The lifetime evolution study of the material, notched, is carried out in two stages:

a) Specimen preparation:

They are sandblasted during eight hours, Fig. 11. The geometry of the notch profile before and after sandblasting is measured, Fig. 12. The form and parameters of the notch are completely changed.

b) Realization of fatigue test:

Roman tile specimens used in fatigue test are subjected to a sinusoidal loading and for a load ratio of 0.5 (the daily evolution of the internal pressure of these pipelines is between 40 and 70 bar). The average load applied is between 750 and 2625 N. This load is applied on the opposite surface to the notch and just in the middle of the horizontal distance between the two supports (180 mm). The specimen section is of 8.8 mm × 15 mm, Fig. 10.

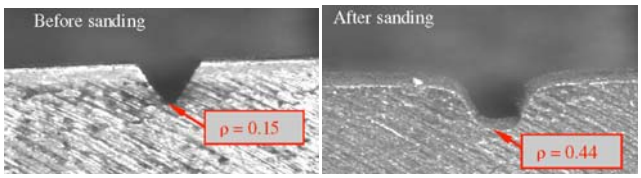


Figure 12. Notch profile geometry before and after sandblasting.
Slika 12. Profil zareza pre i posle peskiranja

The cycle frequency is between 1.7 and 10 Hz for the tests in air, and kept constant at 0.05 Hz for the tests in hydrogen. In the air, it is possible to change the frequency from one test to another, which is not the case in other environments, especially in the corrosion test, /38/. The hydrogen effect, like all corrosion phenomena, needs time to penetrate and affect the steel, /39/. It must be assured that the rupture is not entirely due to mechanical solicitations of the specimen.

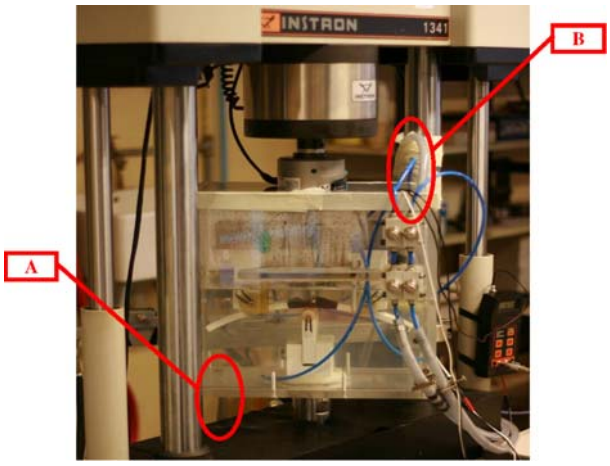


Figure 13. Assembly of 3 points bending test under hydrogen.
Slika 13. Sklop ispitivanja savijanjem u 3 tačke sa vodonikom

For the fatigue tests in hydrogen, a cell with Plexiglas (Fig. 13) is added in relation to the reference configuration in air. The primary function of this cell is to immerse the specimen in the electrolytic solution (NS4) during the test. The electrolytic solution homogeneity is provided by a pump that sucks the solution at point A and pumps it back to point B. Figure 6 represents the hydrogen charging cell of fatigue specimens. By using reference and sandblasted specimens, fatigue tests in hydrogen are carried out. The production of hydrogen is made continuously at the notch level during all the fatigue test period. Sequence of damage (sandblasting + hydrogen, hydrogen + sandblasting or the simultaneous influence of sandblasting and hydrogen) of the steel can lead to different consequences from the viewpoint of mechanical properties. In this paper, we are interested to study the lifetime evolution of material firstly sandblasted and then affected by hydrogen. The goal is to estimate the possibility to use the pipelines network damaged by sandblasting to transport hydrogen.

Wöhler curves obtained from 3-point bending tests, for different cases, are presented in Fig. 14. These curves show that sandblasting increases the life duration and hydrogen decreases it. The beneficial effect of sandblasting is due to three main parameters:
i) Local hardening,
ii) Residual stresses are in compression under the notch,
iii) Notch radius increases during sandblasting. After 8 hours of sanding, the radius increased from 0.15 to 0.44 mm, Fig. 12.

The gain in the material lifetime by sandblasting, compared with the reference one (fatigue test in air carried out to reference specimens), is a function of applied load. This value varies from 32% at the highest load (more than 2250 N) to 143% for a load less than 1000 N.

By comparing the lifetime curve under hydrogen with the other one in air, we noticed that hydrogen is very harmful to the material life. It causes its reduction to 81% for a load of 1688 N and to 58% for a load of 1238 N. During the three point bending test in hydrogen, the large density of dislocations in the middle of specimen, where stresses are highest, act as a trap for hydrogen. The severe drop in material lifetime is due to the presence of hydrogen inside steel that causes the embrittlement of material so that a small effort is sufficient to create cleavage.

Concerning the material affected by hydrogen and sand impacting, lifetime depends on the applied load. For a high load, lifetime decreases (Fig. 14); it is –55% for a load of 2250 N. The more the applied loading decreases, the less important is the drop in lifetime. From a load of 1500 N, life duration is equivalent to that obtained for a specimen tested in air. The combined effect of hydrogen and sandblasting is then cancelled.

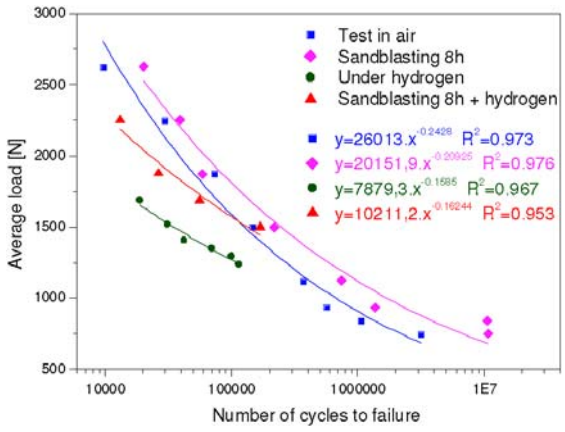


Figure 14. Wöhler curves for pipeline API 5L X52 steel.
Slika 14. Velerove krive čelika za cevovod API 5L X52

*Failure mode*

The variation of lifetime of pipeline API 5L X52 steel, charged with hydrogen and eroded by sandblasting, is due to material damage. In order to observe these changes, a scanning electron microscope (SEM) is used. Figures 15 and 16 illustrate the crack formation in the material.

In air: Classical Cracks create and propagate in the plan. It has been shown to be an important cleavage and the failure seems to be intra granular.

After charging in hydrogen: Cracks initiate in privileged sites outside of cracking plane. The crack follows the porosity path. A small effort is sufficient to create surfaces. There is no distinct direction of crack propagation. The propagation seems to be mixed.

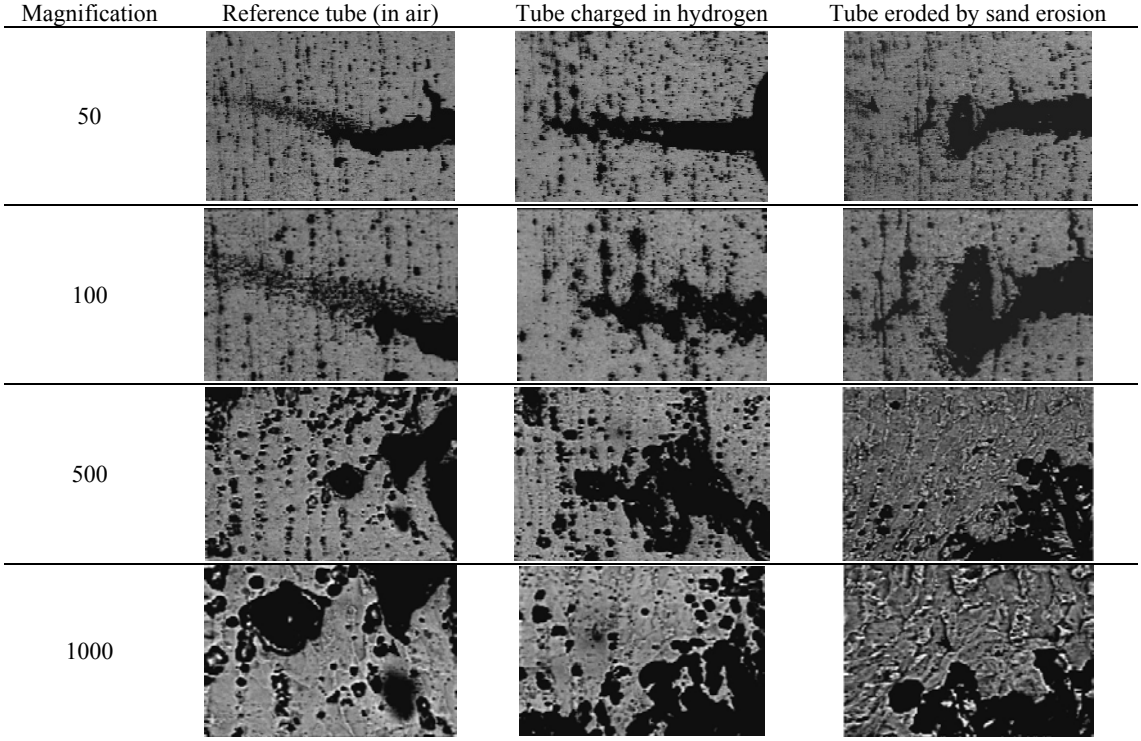


Figure 15. Crack formation in pipeline during its service in different environments: air, hydrogen and sandblasting (SEM).
Slika 15. Nastanak prslina u cevovodu u toku veka rada, u raznim sredinama: vazduh, vodonik i peskiranje (SEM)

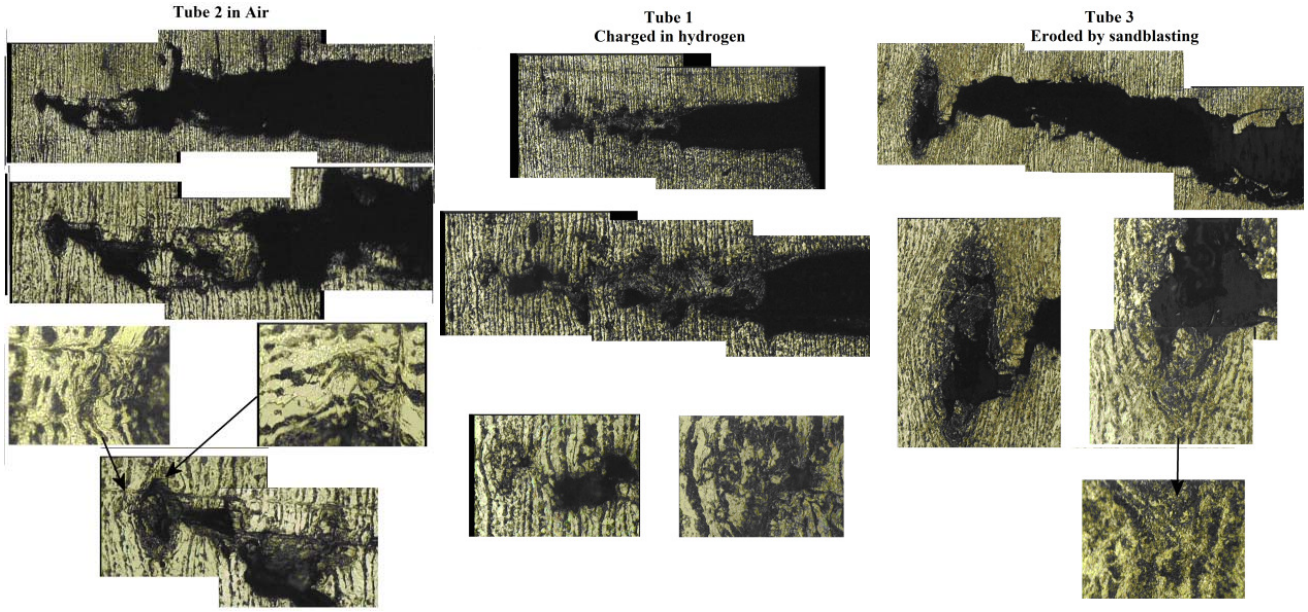


Figure 16. Observation of crack propagation in material by optical microscopy (after chemical treatment with Nital).
Slika 16. Posmatranje rasta prsline u materijalu optičkom mikroskopijom (posle nagrizanja Nitalom)

After sand erosion: Cracks initiate in privileged sites outside of the cracking plane. The deformation field is very important. The crack propagation and the failure seem to be intra granular. We notice a flow of material where deformations are very large.

## FAILURE ASSESSMENT DIAGRAM (FAD)

### *On the use of fatigue initiation threshold in a FAD*

All elasto-plastic failure is characterized by a point in a diagram named Failure Assessment Diagram (FAD). This diagram accounts for any kinds of failure: plastic collapse as well as brittle fracture and elastic-plastic failure, Fig. 17. The FAD exhibits a failure curve as the critical non-dimensional Notch Stress Intensity Factor $K_{\rho,r}$ versus non-dimensional stress or loading parameter $S_r$ and has been applied into several codes in conjunction with the structural integrity structures. The interpolation between 2 limits state (brittle fracture and plastic collapse), is obtained by a curve representing the fracture limit, called Failure Integrity Line.

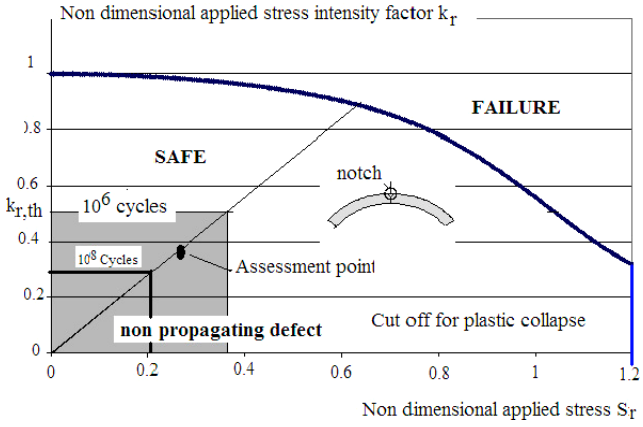


Figure 17. Classical failure assessment diagram with conditions for non-propagating defect.
Slika 17. Klasičan dijagram procene loma sa uslovima za grešku koja se ne širi.

Many interpolation curves have been proposed. We have chosen to use the curve given by the SINTAP procedure. The mathematical expressions of SINTAP default level procedure with the aforementioned assumption can be written as below, /40, 41/:

$$f(S_r)=\left[1+\frac{S_r^2}{2}\right]^{-1/2}\left[0.3+0.7e^{-0.6\cdot S_r^6}\right] \quad \text{for } 0\le S_r\le 1$$

$$\text{and } S_r^{\max}=1+\left(\frac{150}{\sigma_Y}\right)^{2.5}$$

where $f(S_r)$, $S_r$, $S_r^{\max}$ and $\sigma_Y$ are interpolating function, non-dimensional loading or stress based parameter, the maximal value of non-dimensional loading or stress based parameter and yield stress, respectively.

In the Modified Notch Failure Assessment Diagram (MNFAD), the parameters of the MFAD are the following:

$$K_r=K_{\rho,app}/K_{\rho,c}\ ;\ \ S_r=\sigma_{\theta\theta}/\sigma_0$$

where $K_{\rho,app}$, $K_{\rho,c}$, $\sigma_{\theta\theta}$, $\sigma_0$, are respectively: applied Notch Stress Intensity Factor (NSIF), Critical Notch Stress Intensity factor or fracture toughness, hoop stress, reference stress.

It is interesting to connect the Failure Assessment Diagram with the fatigue resistance initiation diagram. This is easily made because the fatigue initiation parameter is also expressed in terms of Notch Stress Intensity Factor. Similarly, we define the non-dimensional threshold Notch Stress Intensity Factor $k_{r,th}$:

$$k_{r,th}=k_{\rho,th}/k_{\rho,c}$$

Its value depends on conventional definition of number of cycles of non fatigue initiation $N_{ni}$. The notch fracture toughness of API 5L X52 has been measured after hydrogen absorption. Its value is equal to 65.73 MPa√m. On Fig. 17, the Modified Notch Failure Assessment Diagram ($K_r$,$S_r$) is drawn. The assessment point which characterized the loaded structure with a notch defect type is reported. The loading path is also drawn and corresponds to a straight

line passing through origin and assessment point, because parameters $K_r$ and $S_r$ are proportional.

*Results*

The notch fracture toughness of pipeline API 5L X52 steel is obtained for reference, impacted by sand and charged by hydrogen specimens. Its values are equal to 69.25 MPa√m, 75.83 MPa√m and 65.73 MPa√m in respect.

Figure 18 presents the modified notch failure assessment diagram ($K_{\rho,r}$; $S_r$). It illustrates the influence of hydrogen and sandblasting on the pipeline API 5L X52 steel. Two zones are defined: Safety zone (if the assessment point is outside of this zone, failure is probable) and security zone (failure probability is of $10^{-5}$).

According to the applied load and the service conditions, it is shown that the three assessment points are inside the security zone. So for the studied notch defect, there is no danger of material lifetime for any working environment (air, hydrogen or sandblasting).

Table 6 gives the values of safety and security factors in the working environment (air, hydrogen and sandblasting) which are calculated by the following equations:

Safety factor: $F_{sf} = \mathrm{OC/OA}$

Safety factor: $F_{sc} = \mathrm{OB/OA}$

For the applied loads on pipeline (service pressure is 70 bar), these factors are acceptable.

Table 6. Influence of hydrogen and sandblasting on the safety and security factors.
Tabela 6. Uticaj vodonika i peskiranja na faktore sigurnosti i bezbednosti

| Safety factor | | | | |
|---|---|---|---|---|
| Air | Hydrogen | Influence | Sandblasting | Influence |
| 2.81 | 2.61 | –7.27% | 2.73 | –2.72% |
| Security factor | | | | |
| Air | Hydrogen | Influence | Sandblasting | Influence |
| 1.89 | 1.76 | –6.67% | 1.89 | 0.10% |

## CONCLUSIONS

The damage of a notched API 5L X52 pipeline steel, under sand impacting and hydrogen effect, is studied. The material lifetime and static properties are evaluated by performing tensile and fatigue 3-point bending tests. Failure mode is observed by a Scanning Electron Microscope and the danger of the studied notch is evaluated by the Failure Assessment Diagram.

One of the first effects of sandblasting and hydrogen on pipeline API X52 steel is the significant variation of the elongation at rupture. In the T direction, it is reduced by 42% in hydrogen and increased 16.8% after sandblasting. The yield stress and ultimate strengths are slightly affected. Generally, these remarks can be considerable whatever the configuration directions of the pipeline are: longitudinal or transverse.

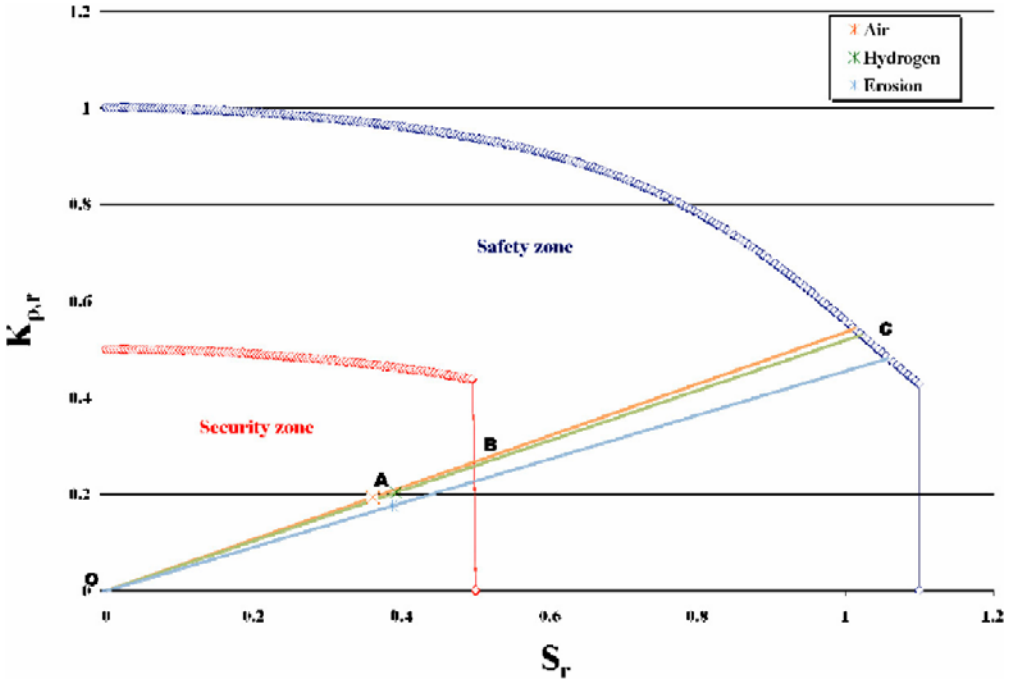


Figure 18. Modified notch failure assessment diagram.
Slika 18. Modifikovani dijagram procene loma sa zarezom

For fatigue, sand erosion improves the life duration of the pipeline, but hydrogen reduces it (it was reduced 73% for a load of 1400 N). The material lifetime under the influence of sand erosion and hydrogen depends on the applied load. The higher the load, the more important is the drop in lifetime. For low loads, it is remarkable that the fatigue curve of the pipeline API 5L X52 steel sandblasted and charged with hydrogen, is relatively similar to that obtained in the air. This is justified by the little deformations equivalent to that in the air.

The cracks initiate and propagate differently through the thickness of a pipe. Hydrogen and sandblasting influence the failure mechanism. It seems following the porosity path and to be intra granular, respectively. For the studied notch with a depth of 20% of pipe thickness, there is no danger of material lifetime.

## REFERENCES


1. Hasan, F., Iqbal J., *Consequential rupture of gas pipeline*, Engineering Failure Analysis 2006; 13: 127-135.
2. Hattori, S., Nakao, E., *Cavitation erosion mechanisms and quantitative evaluation based on erosion particles*, Wear 2002; 249: 839-845.
3. Wood, R.J.K., Puget, Y., Trethewey, K.R., Stokes, K., *The performance of marine coatings and pipe materials under fluid-borne sand erosion*, Wear 1998; 219: 46-59.
4. Bouzid, S., Nyoungue, A., Azari, Z., Bouaouadja, N., Pluvinage, G., *Fracture criterion for glass under impact loading*, Int J of Impact Eng 2001; 25: 831-845.
5. Bozzini, B., Ricotti, M.E., Boniadri, M., Mele, C., *Evaluation of erosion-corrosion in multiphase flow via CFD and experimental analysis*, Wear 2003; 255: 237-245.
6. Nyoungue, A., Azari, Z., Abbadi, M., Dominiak, S., Hanim, S., *Glass damage by impact spallation*, Mater Sci and Eng A 2005; 407: 256-264.
7. Azouaoui, K., Rechak, S., Azari, Z., Benmedakhene, S., Laksimi, A., Pluvinage, G., *Modelling of damage and failure of glass/epoxy composite plates subject to impact fatigue*, Int J of Fatigue 2001; 23: 877-885.
8. Meng, H.C., Ludema, K.C., *Wear models and predictive equations: their form and content*, Wear 1995; 181-183: 443-457.
9. Lillamand, I., Evolution d'une couche grenaillée sous sollicitations thermiques et mécaniques, cas de la fatigue oligocyclique. Thèse ENSAM 1998.
10. Devignes, M., Influence du grenaillage de précontrainte sur la tenue en fatigue de l'acier 35CD4. Thèse ENSAM 1987.
11. Kirk, D., Render, P.E., *Effects of peening on stress corrosion cracking in carbon steel*, Proc. of ICSP7-1999, Warsaw, Poland.
12. De Los Rios, E.R., Artamanov, M., Rodopoulos, C.A., Peyre, P., Levers, A., Proc. of 4th Int. Committee on Aeronautical Fatigue, Toulouse 2001, p.25-29.
13. Vo, L.D., Stephens, R.I., *Effect of Shot and Laser Peening on SAE 1010 Steel Tubes with a Transverse Center Weld Subjected to Constant and Variable Amplitude Loading*, Proc. of 12th Int Conf on Fracture 2009, Canada.
14. Fernandes, T.R.C., Chen, F., da Graça Carvalho, M., *"Hy Society" in support of European hydrogen projects and EC policy*, Int J of Hydrogen Energy 2005; 30: 239-245.
15. Mulder, G., Hetland, J., Lenaers, G., *Towards a sustainable hydrogen economy: Hydrogen pathways and infrastructure*, Int J of Hydrogen Energy 2007; 32: 1324-1331.
16. Hanneken, J.W., *Hydrogen in metals and other materials: a comprehensive reference to books, bibliographies, workshops and conferences*, Int J of Hydrogen Energy 1999; 24: 1005-1026.
17. Dayal, R.-K., Parvathavarthini, N., *Hydrogen embrittlement in power plant steels*, Sadhana 2003; 28: 431- 451.
18. Sofronis, P., Liang, Y., Aravas, N., *Hydrogen induced shear localisation of the plastic flow in metals and alloys*, Eur J of Mechanics / Solids 2001; 20: 857-872.
19. Delafosse, D., Magnin, T., *Hydrogen induced plasticity in stress corrosion cracking of engineering systems*, Eng Fra Mechs 2001; 68: 693-729.
20. Steigerwald, E.A., Schaller, F.W., Traiano, A.R., Trans Metall Soc AIME 1960; 218: p.832.
21. Oriani, R.A., Corrosion 1987; vol. 43, n°7, p.390.
22. Delafosse, D., Bayle, B., Bosch, C., *The roles of crack-tip plasticity, anodic dissolution and hydrogen in SCC of mild and C-Mn steels*, Environment-Induced Cracking of Materials 2008; pp.267-278.
23. Qiao, L.J., Luo, J.L., Mao, X., Corrosion 1998; vol. 54, n°2, p.115-120.
24. Lunarska, E., Ososkov, Y., Jagodzinsky, Y., *Correlation between critical hydrogen concentration and hydrogen damage of pipeline steel*, Int J of Hydrogen Energy 1997, 22: 279-284.
25. Torres-Islas, A., Salinas-Bravo, V.M., Albarran, J.L., Gonzalez-Rodriguez, J.G., *Effect of hydrogen on the mechanical properties of X-70 pipeline steel in diluted $NaHCO_3$ solutions at different heat treatments*, Int J of Hydrogen Energy 2005; 30: 1317-1322.
26. Scoot, X., Mao, Li, M., *Mechanics and thermodynamics on the stress and hydrogen interaction in crack tip stress corrosion: experiment and theory*, J Mech Phys Solids 1998; 46: 1125-1137.
27. Razzini, G., Cabrini, M., Maffi, S., Mussati, G., Peraldo Bicelli, L., *Photoelectrochemical visualization in real-time of hydrogen distribution in plastic regions of low-carbon steel*, Corrosion Science 1999; 41: 203-208.
28. Bastien, P., Azou, P., *Influence de l'écrouissage sur le frottement intérieur de fer et de l'acier, chargé ou non en hydrogène*, C. R. Ac. Sc. 1951 ; 232, Paris, p.1845.
29. Brass, A., Chene, J., Coudreuse, L., *Fragilisation des aciers par l'hydrogène: étude et prévention*, Les Techniques de l'Ingénieurs, M175, 2000.
30. Cheng, Y.F., *Analysis of electrochemical hydrogen permeation through X-65 pipeline steel and its implications on pipeline stress corrosion cracking*, Int J of Hydrogen Energy 2007; 32: 1269-1276.
31. Morales-Gil, P., Negrón-Silva, G., Romero-Romo, M., Ángeles-Chávez, C., Palomar-Pardavé, M., *Corrosion inhibition of pipeline steel grade API 5L X52 immersed in a 1 M $H_2SO_4$ aqueous solution using heterocyclic organic molecules*, Electrochimica Acta 2004; 49: 4733-4741.
32. Capelle, J., Gilgert, J., Dmytrakh, I., Pluvinage, G., *Sensitivity of pipelines with steel API X52 to hydrogen embrittlement*, Int J of Hydrogen Energy 2008; 33: 7630-7641.
33. Capelle, J., Dmytrakh, I., Pluvinage, G., *Comparative assessment of electrochemical hydrogen absorption by pipeline steels of different strength*, Corrosion Science 2010; 52: 1554-1559.
34. NF A 03-001, NF EN 10002-1. Essai de traction, Partie 1: Méthode d'essai (à la température ambiante). AFNOR 1990.
35. Moustabchir, H., Azari, Z., Hariri, S., Dmytrakh, I., *Experimental and numerical study of stress–strain state of pressurised cylindrical shells with external defects*, Eng Fail Anal 2010; 17: 506-514.
36. Hadj Meliani, M., Azari, Z., Pluvinage, G., Matvienko, Yu.G., *The effective T-stress estimation and crack paths emanating from U-notches*, Eng Fract Mechs 2010; 77: 1682-1692.
37. Hadj Meliani, M., Azari, Z., Pluvinage, G., Capelle, J., *Gouge assessment for pipes and associated transferability problem*, Eng Fail Anal 2010; 17: 1117-1126.
38. Zhongping, Y., Zhaohua, J., Xuetong, S., Shigang, X., Zhendong, W., *Influence of the frequency on the structure and corrosion resistance of ceramic coatings on Ti–6Al–4V alloy produced by micro-plasma oxidation*, Mater Chem and Phys 2005; 92: 408-412.
39. International Standard ISO 7539-9. Corrosion of metals and alloys – Stress corrosion testing, Part 9: Preparation and use of pre-cracked specimens for tests under rising load or rising displacement, 2003.
40. Cheng, Y.F., *Fundamentals of hydrogen evolution reaction and its implications on near neutral pH stress corrosion cracking of pipelines*, Electrochimica Acta 2007; 52:2661-7.
41. Capelle, J., Gilgert, J., Pluvinage, G., *A fatigue initiation parameter for gas pipe steel submitted to hydrogen absorption*, Int J of Hydrogen Energy 2010; 35: 833-843.
42. Bouzid, S., Azari, Z., Dominiack, S., Gilgert, J., *Dhieb Glass damages caused by sand impact: evaluation of the eroded volume*, VERRE Volume 9 n°3 2003; 12-20.